Nuclear import of APOBEC3F-labeled HIV-1 preintegration complexes

Ryan C. Burdick[a], Wei-Shau Hu[b], and Vinay K. Pathak[a,1]

[a]Viral Mutation Section and [b]Viral Recombination Section, HIV Drug Resistance Program, Center for Cancer Research, National Cancer Institute, Frederick, MD 21702

Edited* by Stephen P. Goff, Columbia University College of Physicians and Surgeons, New York, NY, and approved October 28, 2013 (received for review August 23, 2013)

Human cytidine deaminases APOBEC3F (A3F) and APOBEC3G (A3G) are host factors that incorporate into virions and restrict virus replication. We labeled HIV-1 particles with yellow fluorescent protein (YFP)-tagged APOBEC3 proteins and examined their association with preintegration complexes (PICs) in infected cells. Labeling of PICs with A3F-YFP, and to a lesser extent A3G-YFP, could be used to visualize PICs in the nuclei, which was dependent on nuclear pore protein Nup153 but not TNPO3. We show that reverse transcription is not required for nuclear import of PICs, indicating that a viral core uncoating event associated with reverse transcription, and the central DNA flap that forms during reverse transcription, are not required for nuclear import. We also quantify association of cytoplasmic PICs with nuclear envelope (NE) and report that capsid mutations that increase or decrease core stability dramatically reduce NE association and nuclear import of PICs. In addition, we find that nuclear PICs remain close to the NE and are not distributed throughout the nuclei. These results provide tools for tracking retroviral PICs in infected cells and reveal insights into HIV-1 replication.

retrovirus | microscopy | early events

APOBEC3G (A3G), APOBEC3F (A3F), and APOBEC3C (A3C) belong to a family of seven DNA cytidine deaminases that exhibit broad antiviral activities (reviewed in ref. 1). A3G and A3F are the most potent inhibitors of HIV type-1 (HIV-1) replication in the absence of the viral infectivity factor (Vif) protein (2, 3), whereas A3C is a potent inhibitor of Vif-deficient simian immunodeficiency virus but not Vif-deficient HIV-1 (4). Vif binds to A3G and A3F in the virus producer cell and targets them for polyubiquitination and proteosomal degradation. A3G and A3F are incorporated into assembling Vif-deficient virions, and upon infection of the target cell, inhibit viral replication by inducing lethal G-to-A hypermutation, obstructing viral DNA synthesis, and hindering viral DNA integration (reviewed in ref. 1).

Although much is known about the antiviral activity of the APOBEC3 (A3) proteins, to date there have been no studies that have analyzed their association with viral reverse transcription complexes (RTCs) or preintegration complexes (PICs) in infected cells using fluorescent microscopy. Some A3G/A3F must remain associated with the RTCs during DNA synthesis, because minus-strand DNA is the substrate for A3G/A3F-mediated cytidine deamination. Moreover, it has been shown that A3F and A3G both inhibit provirus formation, but they do so by different mechanisms; in the presence of A3G, an aberrant viral DNA end is generated as a result of incomplete removal of the tRNA primer, whereas in the presence of A3F, the 3′ processing reaction (removal of two nucleotides from the 3′ ends of DNA) catalyzed by integrase (IN) is inhibited (5, 6). We previously reported that A3F expressed in transfected 293T cells exhibits a higher affinity for dsDNA than A3G in vitro (6). This observation led us to hypothesize that A3F might remain associated with PICs longer than A3G, because after reverse transcription, PICs are expected to contain mostly dsDNA (7).

Here, we demonstrate that A3F-yellow fluorescent protein (YFP), and to a lesser extent A3G-YFP, can be used to label infectious HIV-1 particles and visualize viral PICs in the infected cells, including their nuclei. Reverse transcription was not required for nuclear import of A3F-YFP labeled particles, which colocalized with viral RNA. Mutations in capsid (CA) that decreased or increased viral core stability reduced the accumulation of A3F-YFP–labeled particles at the nuclear envelope (NE) as well as their nuclear import, suggesting that these mutations affected PIC cytoplasmic transport and/or stable association with the NE. We also quantified nuclear penetration of PICs and found that nuclear PICs remained close to the NE and were not distributed throughout the nuclei. Overall, these studies offer insights into the early stage of HIV-1 replication, the biology of virally incorporated A3 proteins, and provide tools to track viral RTCs and PICs from membrane fusion to the nucleus.

Results

Characterization of YFP-Labeled HIV-1 Particles. We transfected an HIV-1-derived-vector (HDV-EGFP), vesicular stomatitis virus envelope glycoprotein (VSV-G), and S15-mCherry expression plasmids along with different amounts of plasmids expressing WT A3G-YFP, A3F-YFP, A3C-YFP, the amino-terminal RNA-binding domain of the P22 bacteriophage N protein fused to YFP (hereafter referred to as P22-YFP), and cytidine deaminase-deficient mutants A3G*-YFP and A3F*-YFP (Fig. 1*A*) to generate virions with similar average YFP particle intensities, although the average intensity of A3C-YFP particles was slightly lower (Fig. 1*B*). The P22 RNA-binding peptide has high specificity for binding

Significance

We observed that fluorescent protein-tagged host restriction factors APOBEC3F (A3F) and APOBEC3G (A3G) remain associated with HIV-1 preintegration complexes (PICs) in the nuclei of infected cells. Using A3F labeling as a tool to visualize PICs, we determined that (*i*) reverse transcription is not required for nuclear import of PICs, indicating that a viral core uncoating event associated with reverse transcription, and the central DNA flap that forms during reverse transcription, are not required for nuclear import; (*ii*) viral core stability mutations dramatically reduce association of PICs with the nuclear envelope as well as diminish their nuclear import; and (*iii*) most nuclear PICs remain close to the nuclear envelope and are not distributed throughout the nuclei.

Author contributions: R.C.B., W.-S.H., and V.K.P. designed research; R.C.B. performed research; R.C.B., W.-S.H., and V.K.P. analyzed data; and R.C.B., W.-S.H., and V.K.P. wrote the paper.

The authors declare no conflict of interest.

*This Direct Submission article had a prearranged editor.

Freely available online through the PNAS open access option.

[1]To whom correspondence should be addressed. E-mail: vinay.pathak@nih.gov.

This article contains supporting information online at www.pnas.org/lookup/suppl/doi:10.1073/pnas.1315996110/-/DCSupplemental.

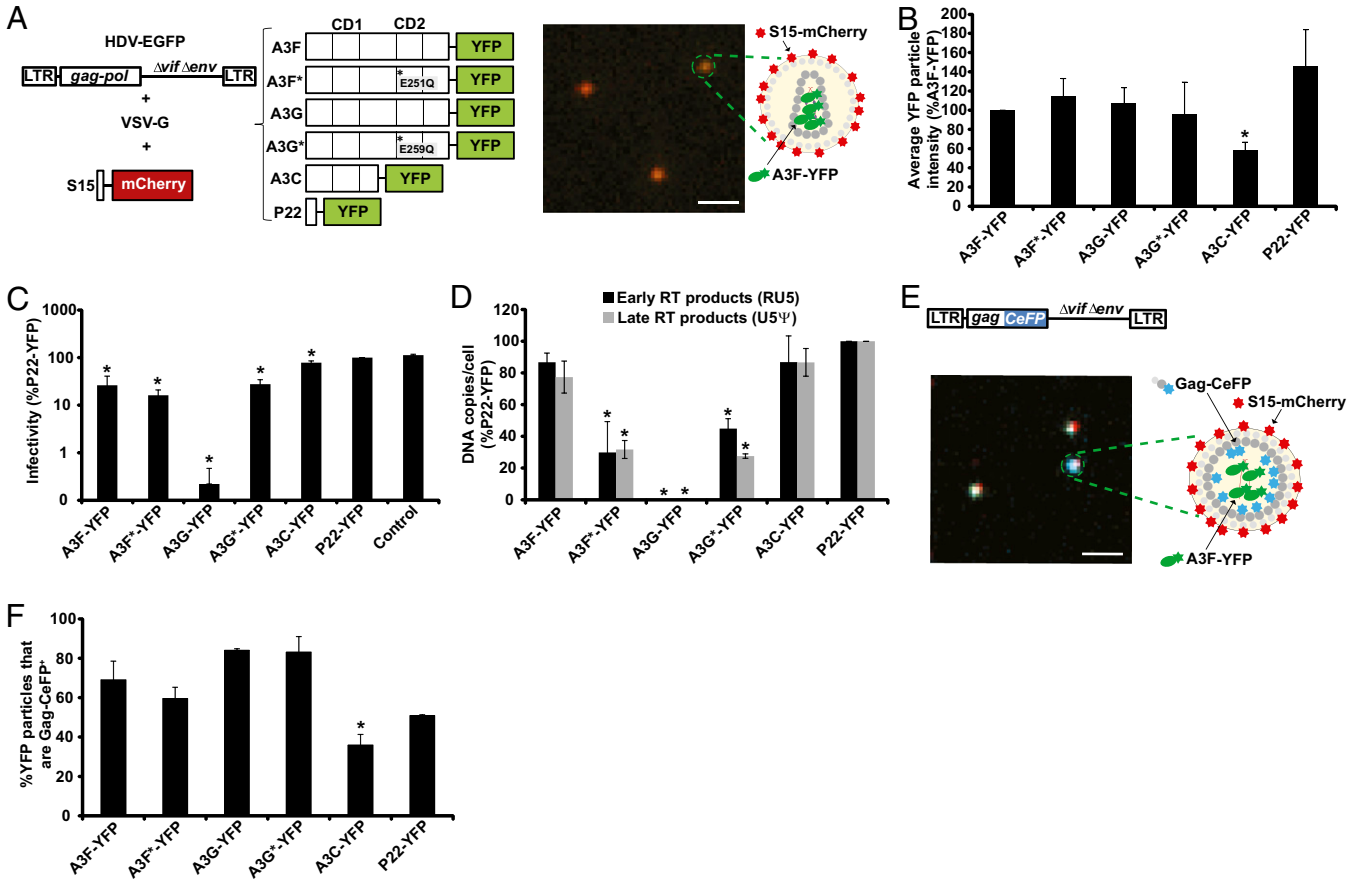

Fig. 1. Detection of single HIV-1 particles using YFP-tagged A3 proteins or a YFP-tagged P22 RNA binding peptide. (*A*) (*Left*) Schematics of the constructs used to produce VSV-G pseudotyped HIV-1 particles that are labeled with the S15-mCherry membrane marker and various YFP-tagged proteins. (*Right*) A3F*-YFP and A3G*-YFP contain E251Q and E259Q mutations, respectively, that abolish cytidine deaminase activity. Representative image and schematic of a fluorescently labeled virus particle. (Scale bar, 2 μm.) (*B*) Average integral fluorescence intensity of YFP-labeled particles. Approximately 2,000 particles from three independent virus preparations were analyzed for each sample. A3F-YFP intensity was set to 100%. (*C*) Relative infectivity of the YFP-labeled viruses. The viruses, which express GFP from the *nef* ORF, were used to infect HeLa cells, and the proportion of GFP$^+$ cells was determined by FACS 48 h after infection. Infectivity was then normalized for p24 CA input. (*D*) Effect of YFP-labeled proteins on viral DNA synthesis. HeLa cells were infected with 2.5 ng p24 CA-equivalent virus, and viral DNA early (RU5) and late (U5Ψ) products were quantified 6 h after infection. Host *CCR5* gene copy numbers were determined for normalization of cell numbers. (*E*) (*Upper*) Schematic of the HIV-1 expression vector used to create noninfectious Gag-CeFP labeled particles that are also labeled with S15-mCherry and the various YFP-tagged proteins. (*Lower*) Representative image and schematic of a fluorescently labeled noninfectious virus particle. (Scale bar, 2 μm.) (*F*) Average percentage of YFP particles that are also Gag-CeFP$^+$. Error bars indicate SDs of two to three independent experiments. *$P \leq 0.05$; *t* test.

to the boxB RNA hairpin in vitro (8, 9); however, virion incorporation of packaging defective A3G mutants can be restored upon fusion to the P22 RNA-binding peptide, indicating that the P22 RNA-binding peptide can bind RNA nonspecifically in vivo (10). Compared with the no YFP-labeled protein control, A3C-YFP or P22-YFP expression did not substantially affect virus infectivity (<twofold), A3F-YFP, A3F*-YFP, and A3G*-YFP expression decreased infectivity by ~fivefold, and A3G-YFP expression decreased infectivity by nearly 500-fold (Fig. 1*C*). Thus, with the exception of virions labeled with WT A3G-YFP, the infectivity of virions labeled with YFP-tagged proteins were within fivefold of the unlabeled virions. We analyzed the effects of virion incorporation of the A3 proteins on the efficiency of reverse transcription (Fig. 1*D*). In the presence of WT A3G-YFP, synthesis of early and late reverse transcription products was almost completely inhibited at 6 h after infection. In the presence of A3G*-YFP and A3F*-YFP, a 50–70% decrease in the levels of early and late viral DNA products (relative to P22-YFP–labeled virus) was observed, whereas the levels of early and late viral DNA products for A3F-YFP, A3C-YFP, and P22-YFP were similar. Thus, with the exception of A3F-YFP, the accumulation of early and late viral DNA products at 6 h after infection reflected the overall infectivity of these virions. Because our goal was to produce virus preparations with similar average YFP particle intensity, the amounts of A3-YFP incorporation may not reflect the amounts of these proteins packaged in virions during a natural infection. Therefore, the effect of these proteins on virus infectivity and viral cDNA synthesis reflect these experimental conditions and cannot be extrapolated to a natural infection.

To determine the efficiency with which YFP-labeled proteins were associated with virions, we generated virions in the presence of a plasmid that expresses a Gag-cerulean fluorescent protein (CeFP) fusion protein (Fig. 1*E*). As determined by single-virion fluorescence microscopy (11), most of the A3F- and A3G-YFP labeled particles were Gag-CeFP$^+$ (~60–84%), but some may be nonviral vesicles. The proportion of A3C- and P22-YFP labeled particles that were Gag-CeFP$^+$ was slightly lower (36% and 51%, respectively) (Fig. 1*F*). The efficiency with which virions (Gag-CeFP particles) were labeled was similar for A3F-YFP, A3F*-YFP, A3G-YFP, A3G*-YFP, and P22-YFP (ranging from 48% to 72%) but was lower for A3C-YFP (12%) (Fig. S1*A*). The labeling efficiency of the infectious (HDV-EGFP) could po-

tentially be different from that of noninfectious (Gag-CeFP) viruses. Because of potential differences in A3-YFP labeling efficiency, we infected cells with similar numbers of YFP-labeled particles, and the precise A3-YFP labeling efficiency did not affect the interpretation of our results.

Nuclear Import of A3F-YFP–Labeled Particles. We quantified the number of YFP-labeled particles in each virus preparation and infected HeLa cells with equivalent numbers of particles labeled with each of the YFP-tagged proteins. The cells were fixed immediately after spinoculation, the nuclei were stained with DAPI, and confocal z-stacks were acquired of the whole cells to quantify the number of YFP-labeled particles in the entire cell (Fig. 2*A*). The average number of YFP particles per cell ranged from 76 to 101, similar to the YFP particles/cell ratio used to determine the multiplicity of infection (MOI; Fig. S2*A*). To detect YFP particles in the cells after infection, we infected the cells by spinoculation as in Fig. 2*A*, except that the infected cells were incubated at 37 °C for 3, 6, 12, and 24 h after infection, and the NE was stained with anti-Lamin A/C antibody (Fig. 2*B*). Even though ∼100 particles were attached per cell at the 0-h time point after spinoculation with all YFP-labeled virions, we could only detect ∼50 A3F-YFP and A3F*-YFP labeled particles at the 3-h time point, indicating that ∼50% of the particles became undetectable as a result of their degradation, or dissociation of A3F-YFP and A3F*-YFP from the RTCs/PICs. The numbers of A3G-YFP and A3G*-YFP labeled particles were approximately fivefold lower than the A3F-YFP–labeled particles at the 3-h time point (11 and 8 particles per cell, respectively) and the numbers of A3C-YFP- and P22-YFP–labeled particles were even further reduced at the 3-h time point (4 and 1 particle per cell, respectively). These observations suggest that although some A3F-YFP may dissociate from the RTCs during the first 3 h of infection, A3G-YFP, A3G*-YFP, A3C-YFP, and P22-YFP dissociate more rapidly from the RTCs/PICs.

To determine the proportion of viruses that underwent membrane fusion (i.e., lost the S15-mCherry signal) by our earliest time point (3 h), we infected cells as in Fig. 2*B* but stained the nuclei with DAPI in the absence of Triton X-100 (Fig. 2*C*) before image acquisition. Because the S15-mCherry labeling efficiency of virions was not 100% and varied slightly across samples (Fig. S1*B*), we analyzed the percent decrease in YFP particles that are also S15-mCherry$^+$, of which >95% are virions (Fig. S1*C*). We observed a 93% decrease in the number of YFP particles that were also S15-mCherry$^+$ at 3 h, indicating that the vast majority of virions fused with the endosome membrane by 3 h after infection (Fig. 2*C*).

We also quantified the number of nuclear YFP-labeled particles; a representative z-stack of a nucleus containing A3F-YFP–labeled particles is shown in Fig. 2*D*. Only A3F-YFP and to a lesser extent A3F*-YFP could be detected in the nuclei of infected cells (Fig. 2*E*). The number of nuclear YFP particles increased and peaked at 6 and 12 h for A3F*-YFP (0.5 particles per nucleus) and A3F-YFP (1.5 particles per nucleus), respectively. The loss of >80% of A3G-YFP-, A3G*-YFP-, A3C-YFP-, and P22-YFP–labeled particles from cells at the 3-h time point (Fig. 2*B*) partly explains why PICs labeled by these proteins were not detected in the nuclei of infected cells. When cells were infected with A3F-YFP–labeled viruses prepared in the absence of VSV-G expression, the detection of A3F-YFP particles in the nuclei was reduced 10- to 30-fold (<0.05 particles per nucleus), indicating that membrane fusion is required for detection of A3F-YFP particles in the nuclei of infected cells. The maximum number of A3F-YFP particles in

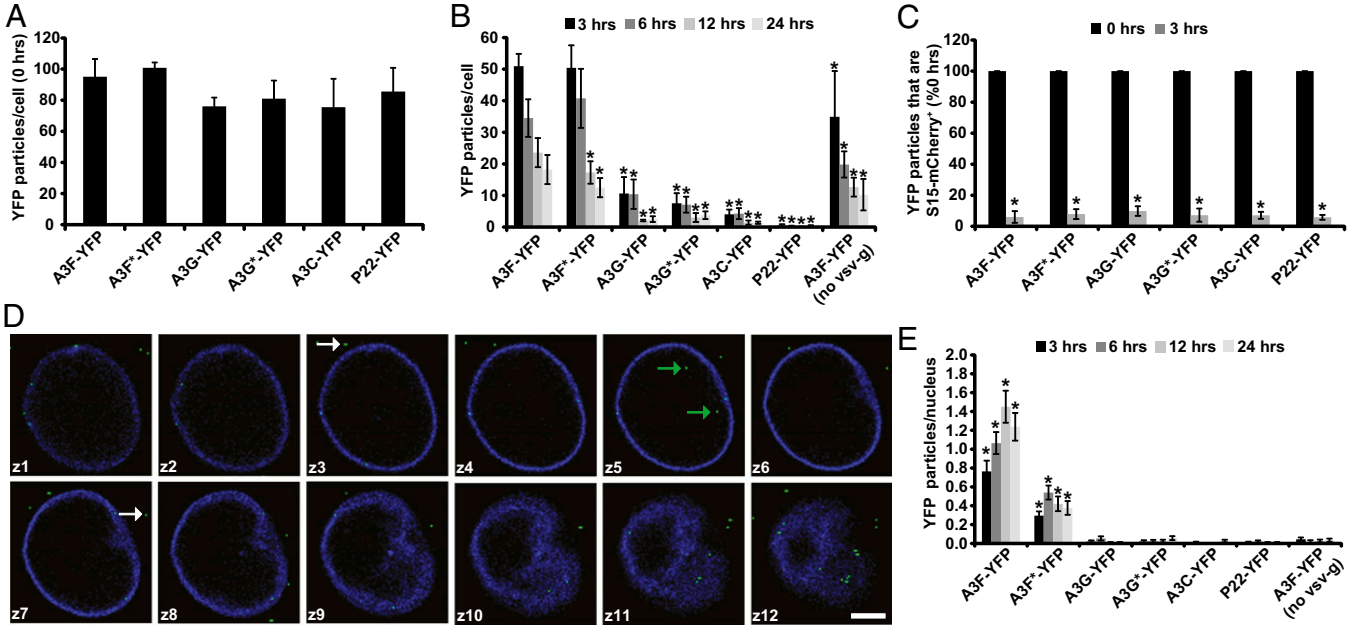

Fig. 2. Detection of A3F- and A3F*-labeled PICs in the nuclei of infected cells. (*A*) Infection of HeLa cells with a normalized number of YFP particles. HeLa cells were infected by spinoculation with a normalized number of YFP-labeled particles and fixed immediately after infection (0 h). Confocal z-stacks were acquired of the entire cells, and the YFP signals were quantified. (*B*) Quantitation of the YFP particles in cells at 3, 6, 12, and 24 h after infection. *Significantly different from the A3F-YFP sample at the respective time point ($P \leq 0.05$; *t* test). (*C*) Quantitation of YFP$^+$ S15-mCherry$^+$ particles at 0 h (set to 100%) and 3 h after infection. Error bars indicate SD. *Significantly different from the 0-h time point ($P \leq 0.05$; *t* test). (*D*) Representative confocal z-stack of a HeLa cell infected with A3F-YFP–labeled virus particles 6 h after infection. The NE was immunostained using an anti-Lamin A/C antibody followed by an Alexa Fluor 405-labeled secondary antibody (blue). Green arrows indicate A3F-YFP particles inside the nucleus; white arrows indicate A3F-YFP particles outside the nucleus. The labels in each image indicate z-position, where z1 is the bottom of the nucleus and z12 is the top of the nucleus. (Scale bar, 5 μm.) (*E*) Quantitation of the YFP signals in the nuclei of infected cells. HeLa cells infected with a normalized numbers of YFP particles were fixed at various time points, confocal z-stacks were acquired of the entire cells, and nuclear YFP signals were quantified (average of 123 nuclei per sample from two independent experiments). Error bars indicate SEM. *Significantly different from the A3F-YFP (no VSV-G) sample at the respective time point ($P \leq 0.05$; *t* test).

each nucleus (1.5 at 12 h) is similar to the expected MOI (~two GFP-expressing proviruses per cell) (Fig. S2*A*).

Effect of siRNA-Induced Knockdown of Nucleoporin 153 kDa and Transportin 3 on Nuclear Import of A3F-YFP–Labeled Particles. To determine whether the nuclear A3F-YFP particles are viral PICs, we determined the effect of siRNA-mediated knockdown of two well-studied nuclear transport proteins, Nucleoporin 153 kDa (Nup153) and Transportin 3 (TNPO3), on the detection of nuclear A3F-YFP particles. Using siRNAs, we could achieve significant knockdown of Nup153 and TNPO3 in the HeLa target cells (87% and 78%, respectively; Fig. 3*A*). After 48 h of knockdown, these cells were infected with A3F-labeled WT virus that was capable of reverse transcription (RT^+) or virus that contained a catalytic site mutation D110E in reverse transcriptase (RT) that was defective for reverse transcription (RT^-; Fig. 3*B*). Consistent with previous reports, we observed a fivefold decrease in infectivity with Nup153 and TNPO3 knockdown (16% and 20% of WT, respectively) (12–15). As expected, the D110E virus was noninfectious (16). Knockdown of Nup153 or TNPO3 did not affect reverse transcription of WT virus, because the amount of late products per cell was similar to the control siRNA (Fig. 3*C*). We also quantified the number of 2-long terminal repeat (LTR) circles, an indicator of nuclear import, at 24 h after infection and detected a 2.3-fold and 2.7-fold decrease after Nup153 and TNPO3 depletion, respectively, in cells infected with WT virus (Fig. 3*D*); as expected, no late viral DNA products or 2-LTR circles were detectable in cells infected with the D110E virus.

We detected a decrease in the number of nuclear A3F-YFP particles upon Nup153 knockdown with WT virus as well as D110E virus (1.7- and 1.3-fold decreases, respectively; Fig. 3*E*). These results indicate that nuclear import of PICs derived from both WT and D110E virus was at least partially dependent on Nup153. The decrease in WT A3F-YFP particles upon Nup153 knockdown was similar to the decrease in 2-LTR circles (1.7- vs. 2.3-fold decrease, respectively). There was no decrease in the number of nuclear A3F-YFP particles upon TNPO3 depletion in cells infected with WT or D110E virus, consistent with reports indicating that TNPO3 depletion acts on HIV-1 at a step after entry of the PIC into the nucleus (12, 15, 17, 18). The decrease in 2-LTR circles (2.7-fold decrease) upon TNPO3 depletion, but not nuclear import of A3F-YFP particles, indicates that TNPO3 may affect the formation and/or stability of 2-LTR circles, which is consistent with a previous report (15). Overall, these data indicate that nuclear localization of A3F-YFP–labeled particles is partially dependent on Nup153, as has been reported for viral PICs (14, 19), providing strong evidence that nuclear A3F-YFP–labeled particles are viral PICs. The decrease in the nuclear import of A3F-YFP particles upon Nup153 knockdown does not fully account for the greater decrease in infectivity (42% vs. 84%, respectively), indicating that Nup153 knockdown also affects a step in replication after nuclear import. Additional studies are needed to clarify the role of Nup153 in HIV-1 replication and the potential biological relevance of this decrease in nuclear import of PICs.

Colocalization of A3F-YFP and Viral RNA in the Nuclei of Infected Cells. To further verify that the A3F-YFP–labeled particles in the nuclei are PICs, we detected viral RNA by FISH and determined its colocalization with the A3F-YFP signals. HeLa cells were infected with A3F-labeled WT virus in the presence or absence of the RT inhibitor nevirapine (NVP; 5 μM) or with the A3F-labeled D110E virus. Six hours after infection, the NE was immunostained and the viral RNA was detected by in situ hybridization to 48 fluorescent probes that specifically hybridized to the *gag-pol* portion of the viral RNA (Fig. 4*A*). We detected very few viral RNA particles in the nuclei of cells infected with WT virus in the absence of NVP (Fig. 4*B*, *Top*). In contrast, in cells infected with WT virus in the presence of NVP (Fig. 4*B*, *Middle*),

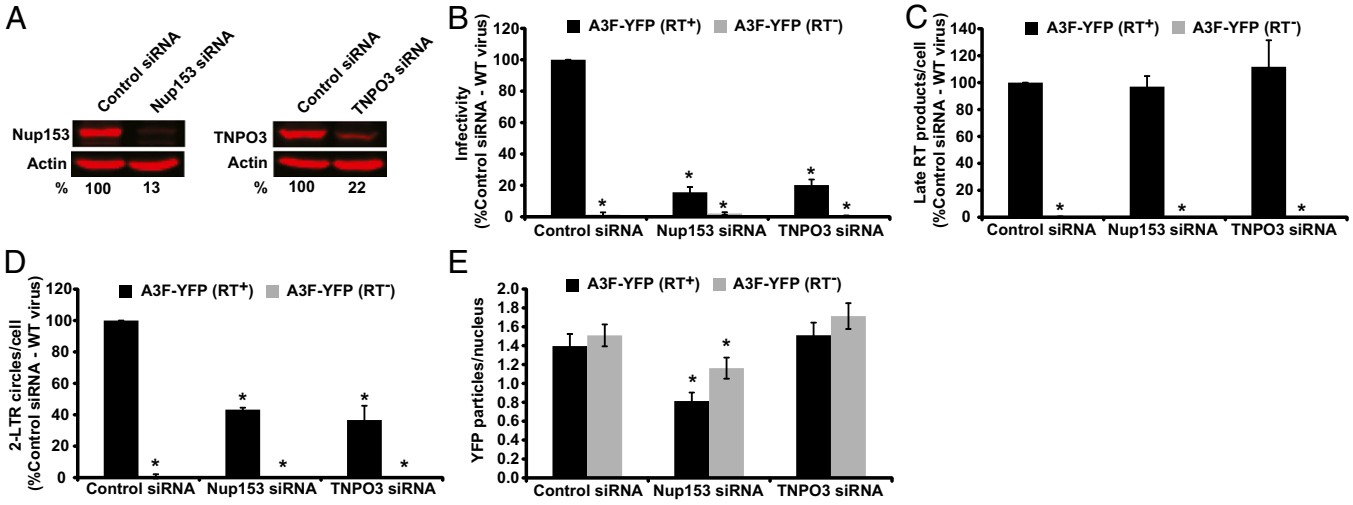

Fig. 3. Nuclear import of A3F-labeled PICs is dependent on Nup153 but independent of TNPO3 and does not require reverse transcription. (*A*) Efficiency of siRNA-mediated knockdown of Nup153 (*Left*) and TNPO3 (*Right*) in HeLa cells. Quantitative immunoblotting analysis of HeLa cells 48 h after transfection with control, Nup153, or TNPO3 siRNAs. The numbers below each lane indicate the percentage of protein remaining after knockdown relative to the siRNA control (average of three independent experiments). The amount of actin detected was used as a loading control. (*B*) Comparison of virus infectivity after Nup153- or TNPO3-depletion in target cells. Infectivity of A3F-YFP–labeled wild-type virus (RT^+) and D110E virus (RT^-) was determined by detection of GFP expression in target cells by FACS 48 h after infection, and the infectivity in control siRNA-treated cells was set to 100%. Error bars indicate SD of two independent experiments. (*C* and *D*) Quantitation of late RT (U5Ψ) and 2-LTR circle products by real-time quantitative PCR 24 h after infection. Host *CCR5* gene copy number was determined and used to normalize cell numbers. Error bars indicate SD of three independent experiments. (*E*) Quantitation of the YFP signals in the nuclei of infected cells 6 h after infection. Nup153- or TNPO3-depleted cells were infected with a normalized number of wild-type (RT^+) or D110E virus (RT^-) YFP-labeled virus particles (same as in *C* and *D*) and fixed 6 h after infection. Confocal *z*-stacks were acquired of the entire cells, and the YFP signals in the nuclei were quantified (average of 173 nuclei per sample from two independent experiments). Error bars indicate SEM. *Significantly different from the respective Control siRNA samples ($P \leq 0.05$; *t* test).

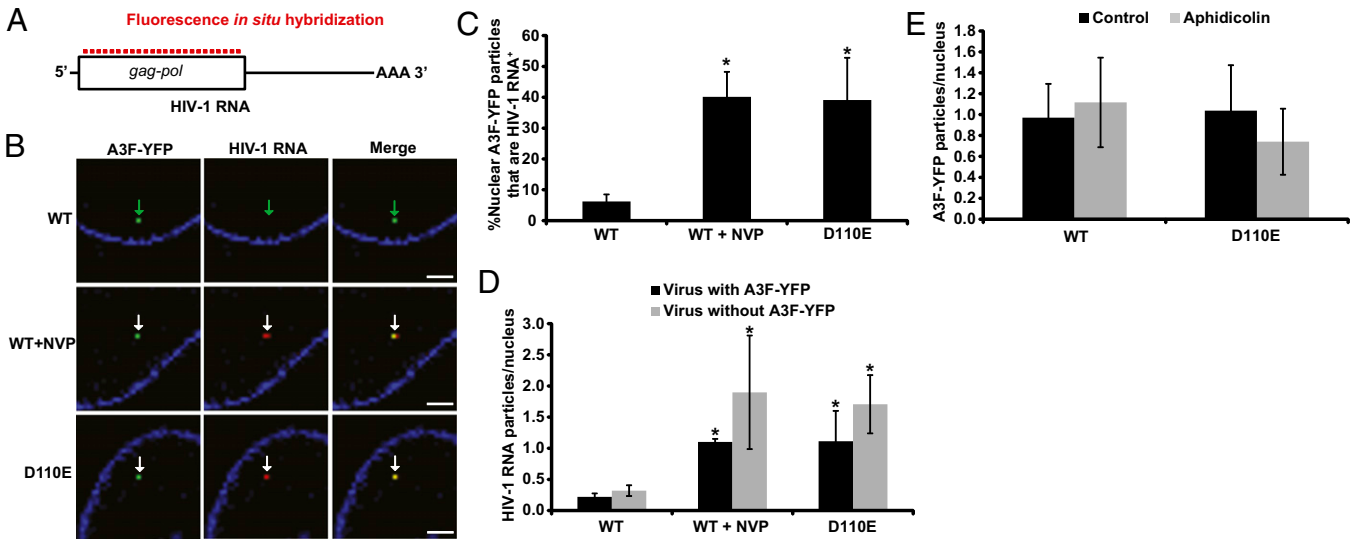

Fig. 4. Nuclear A3F-YFP–labeled PICs colocalize with viral RNA. (*A*) Schematic of the FISH probes used to detect HIV-1 RNA. (*B*) Representative confocal images of A3F-YFP particles in the nuclei of HeLa cells that colocalize with viral RNA 6 h after infection. Infection with wild-type A3F-YFP–labeled virus of HeLa cells treated without (WT) or with 5 μM nevirapine (WT + NVP), or RT$^-$ virus (D110E). The NE was immunostained using an anti-Lamin A/C antibody (followed by an Alexa Fluor 405-labeled secondary antibody; blue), and viral RNA (red) was detected by FISH. Confocal z-stacks were acquired of the entire cells, and the YFP and RNA signals in the nuclei were quantified. Green arrows indicate an A3F-YFP particle that does not colocalize with viral RNA; white arrows indicate A3F-YFP particles that colocalize with viral RNA. Images are from a single slice obtained from a confocal z-stack. (Scale bars, 2 μm.) (*C*) Percentage of nuclear A3F-YFP particles associated with HIV-1 RNA. *Significantly different from the WT sample ($P \leq 0.05$; *t* test). (*D*) Comparison of HIV-1 RNA particles in the nuclei of HeLa cells infected with A3F-YFP labeled particles or viruses that do not contain A3F-YFP. *Significantly different from the WT samples ($P \leq 0.05$; *t* test). (*E*) Quantitation of A3F-YFP particles in the nuclei of untreated or aphidicolin-arrested HeLa cells. Untreated HeLa cells or cells treated with aphidicolin were infected with WT virus or D110E virus and fixed 6 h after infection. Confocal z-stacks were acquired of the entire cells, and the YFP signals in the nuclei were quantified. For *C–E*, ~230 nuclei from three to four independent infections were analyzed for each sample; error bars indicate SD.

or in cells infected with the D110E virus (Fig. 4*B*, *Bottom*), we could readily detect HIV-1 RNA signals in the nuclei, and a larger proportion of these signals colocalized with the A3F-YFP signals. Quantification of the results indicated that only ~6% of the A3F-YFP signals in the nuclei of cells infected with WT virus colocalized with HIV-1 RNA signals, but ~40% of the nuclear A3F-YFP signals colocalized with HIV-1 RNA signals in WT virus-infected cells in the presence of NVP or in cells infected with the D110E virus (Fig. 4*C*). Thus, there was a 6.7-fold increase in the proportion of nuclear A3F-YFP signals that colocalized with HIV-1 RNA when reverse transcription was inhibited by treatment with an RT inhibitor or by a catalytic site mutation in RT. These results are consistent with the expectation that in cells infected with WT virus in the absence of NVP, reverse transcription is nearly complete 6 h after infection (Fig. S2*B* and ref. 20), and most of the viral RNA is likely degraded by the RNase H domain of RT. On the other hand, when reverse transcription is inhibited by NVP, or when cells are infected with the D110E virus, viral RNA is intact and can be detected by FISH, and a large proportion of the RNA signals colocalize with the A3F-YFP signals.

We also quantified the proportion of HIV-1 RNA particles in the nuclei that were A3F-YFP$^+$ (Fig. S3). We observed that ~60% of the HIV-1 RNA particles were A3F-YFP$^+$, which is consistent with the observation that ~50% of the virions are labeled with A3F-YFP (Fig. S1*A*). The results also suggest that the nuclear A3F-YFP does not significantly dissociate from the viral RNA, because dissociation of A3F-YFP from HIV-1 RNA would have further reduced the percentage of HIV-1 RNA particles that were A3F-YFP$^+$. Furthermore, because nuclear A3F-YFP did not significantly dissociate from HIV-1 RNA, the labeling of ~40% of the A3F-YFP with HIV-1 RNA from the viruses that were defective for reverse transcription (Fig. 4*C*) likely reflects the HIV-1 RNA labeling efficiency of our experiments.

We also infected cells with equivalent amounts of p24-CA normalized virus prepared in the presence or absence of A3F-YFP and quantified the number of HIV-1 RNA signals in the nuclei of infected cells (Fig. 4*D*). Although we observed a significant increase in the number of HIV-1 RNA signals in the nuclei of cells infected in the presence of NVP or cells infected with the D110E virus, we did not observe any significant differences in nuclear HIV-1 RNA signals in the presence or absence of A3F-YFP. This result indicated that virion incorporation of A3F-YFP did not significantly influence the nuclear import of viral PICs. Overall, on the basis of the colocalization of HIV-1 RNA and A3F-YFP in the nuclei, along with the dependence of A3F-YFP particles on Nup153 for nuclear import, we conclude that the A3F-YFP signals in the nuclei are PICs.

To determine the effect of cell division on the nuclear import of A3F-labeled PICs, HeLa cells were arrested in the G1/S phase of the cell cycle with aphidicolin treatment (2 μg/mL), an inhibitor of DNA polymerase α (21, 22), and infected with A3F-YFP–labeled WT virus or D110E virus (Fig. 4*E*). The numbers of A3F-YFP signals in the nuclei of infected cells at 6 h after infection were quantified. There was no significant difference in the nuclear import of A3F-labeled PICs in aphidicolin-arrested cells relative to control cells, indicating that the majority of A3F-labeled PICs by 6 h entered the nucleus via active transport across the NE and not during cell division.

Detection of A3G-Labeled PICs Is Less Efficient than A3F-Labeled PICs. Because we did not observe nuclear A3G-labeled PICs by infecting cells using the same amount of virus as A3F-labeled virus (Fig. 2*E*), we sought to determine whether A3G-labeled PICs could be detected in the nuclei of infected cells by increasing the amount of virus used for infection. By using three-fold higher amounts of A3G-labeled virus relative to the A3F-labeled virus, we could detect similar numbers of YFP particles per cell at the 6-h time point (Fig. 5*A*). Next we quantified the A3F-YFP and A3G-YFP signal in the nuclei of infected cells and determined that A3G-labeled particles could be detected with

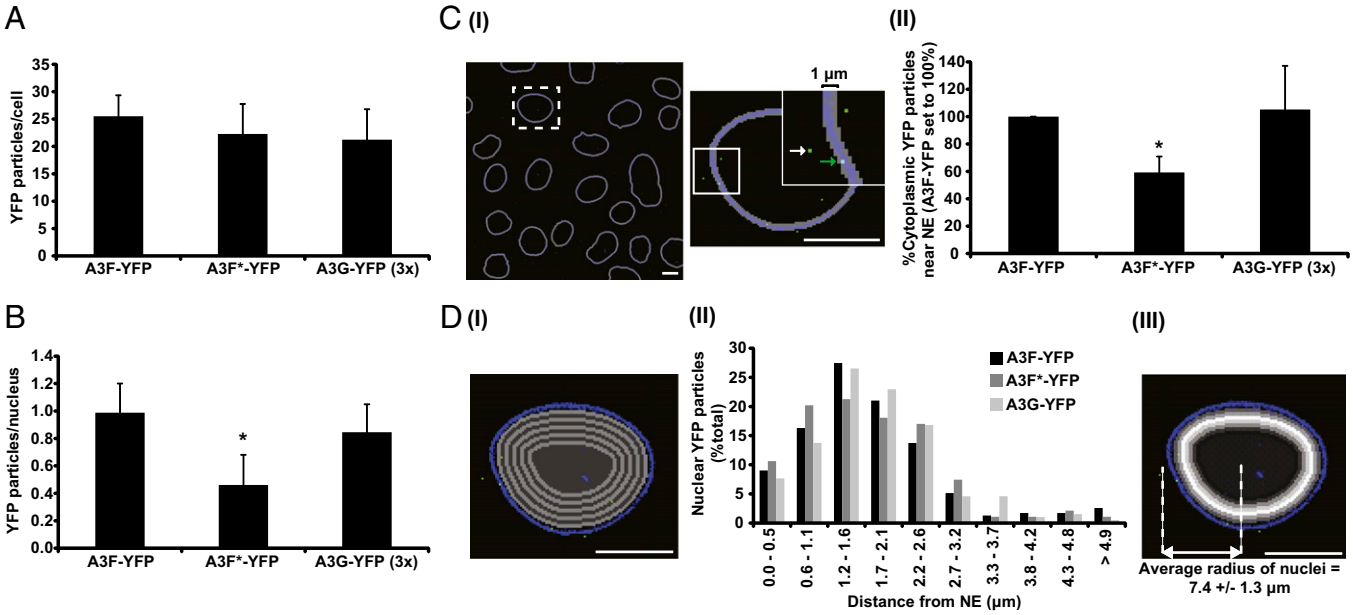

Fig. 5. Detection of A3G-labeled PICs in the nuclei of cells infected with threefold higher amount of virus. (*A*) Quantitation of A3F-, A3F*-, and A3G-YFP labeled particles in cells 6 h after infection. HeLa cells were infected with threefold higher amounts of A3G-YFP–labeled particles compared with A3F-YFP- and A3F*-YFP–labeled particles and fixed at 6 h. Confocal z-stacks were acquired of the entire cells, and the YFP signals were quantified. (*B*) Quantitation of the A3F-, A3F*-, and A3G-YFP signals in the nuclei of infected cells 6 h after infection. *Significantly different from A3F-YFP ($P \leq 0.05$; *t* test). (*C*) Quantitation of cytoplasmic YFP particles associated with the NE. (*i*) The NE was immunostained using an anti-Lamin A/C antibody followed by an Alexa Fluor 405-labeled secondary antibody (blue). A ring 4 pixels in width (~1.0 μm) that includes the area on and immediately surrounding the NE was created (gray), and the percentage of cytoplasmic YFP particles that were in this ring was quantified. A typical image (~20 cells) with an overlay of the mask of the NE and surrounding region (*Left*) and a close-up of a cell that contains particles near the NE (*Right*) is shown. NE-associated (green arrow) and non–NE-associated (white arrow) cytoplasmic A3F-YFP particles are shown. (*ii*) The relative percentage of cytoplasmic YFP particles that is associated with the NE is shown (A3F-YFP set to 100%). An average of 1,464 particles from 270 cells was analyzed per sample. Error bars indicate the SD of four independent experiments. (*D*) Quantitation of nuclear penetration distance for YFP-labeled PICs. (*i*) A series of 9 concentric rings, 2 pixels wide (0.53 μm), inside the nucleus were created starting from the inside edge of the NE, and alternately colored light and dark gray for visualization. (*ii*) YFP particles within each ring were quantified and displayed as a percentage of the total number of nuclear YFP-labeled PICs for each sample (94–233 PICs per sample). (*iii*) The distribution of YFP-labeled PICs in the nuclei is shown by converting the average percentage in each ring to greyscale intensity, with the highest percentage of YFP-labeled particles shown as white and the absence of YFP-labeled particles shown as black. The data from all three samples was pooled to determine the average distribution. The average radius of nuclei was 7.4 ± 1.3 μm. (Scale bars, 10 μm.)

similar efficiency as A3F-labeled particles (Fig. 5*B*). In total, these results indicate that A3G labels PICs less efficiently than A3F, because it was necessary to infect with more viruses to detect similar numbers of particles at the 6-h time point. However, the efficiency of nuclear import and detection of the A3G-labeled particles in the nuclei was similar to that of A3F-labeled particles (compare Fig. 5 *A* and *B*).

Quantitation of Stable Association of PICs with the NE. To further explore the steps immediately before the nuclear import of A3F- and A3G-labeled PICs, we developed an assay to determine viral PIC association with the NE. Briefly, the NE was immunostained using an anti-Lamin A/C antibody followed by an Alexa Fluor 405-labeled secondary antibody. A ring 4 pixels in width (~1.0 μm) that includes the area on and immediately surrounding the NE was created, and the percentage of cytoplasmic YFP particles that were in this ring was quantified as described in *Materials and Methods* (Fig. 5 *C–I*). The percentage of cytoplasmic YFP particles that were associated with the NE for A3F-YFP averaged 24% ± 7%. Samples were normalized to the A3F-YFP sample (set to 100%) to account for variation across experiments. We detected a 1.7-fold decrease in the percentage of A3F*-YFP–labeled cytoplasmic PICs that were associated with the NE relative to A3F-YFP (Fig. 5 *C*, *ii*), which was similar to the 2.2-fold decrease in A3F*-YFP particles per nucleus (Fig. 5*B*). We also estimated that the area of the NE mask contained 8% of the total cytoplasmic area, indicating that more particles are associated with the NE than would be predicted if particles were randomly distributed in the cytoplasm (24% vs. 8%, respectively).

We estimated the efficiency with which a particle that attaches to a cell stably associates with the NE and enters the nucleus. In our experiments, ~100 A3F-YFP labeled particles were attached per cell at the 0-h time point (Fig. 2*A*), of which ~26 A3F-YFP labeled particles were detectable at the 6-h time point (Fig. 5*A*), and ~24% of the particles detectable at the 6-h time point (~6 particles) were stably associated with the NE. Thus, only ~6% of the particles that were attached to the cell were stably associated with the NE, and ~1% of the particles entered the nucleus (Fig. 5*B*). Overall, these results indicate that both stable association of the PICs with the NE and their nuclear import are major barriers to successful infection.

Determination of Nuclear Penetration Distance by PICs. We developed a quantitative assay to determine the nuclear penetration distance for each YFP-labeled PIC. Briefly, a series of nine rings (2 pixels wide; 0.53 μm) inside the nucleus were created starting from the inside edge of the NE toward the center of the nucleus (Fig. 5 *D–I*), and the numbers of YFP-labeled PICs in each ring were quantified (Fig. 5 *D*, *ii*). The distance PICs traveled into the nucleus was similar for all three samples; on average the PICs were located 1.2–1.6 μm from the NE. We also determined that the average nuclear radius was 7.4 ± 1.3 μm and that the majority of PICs typically traveled ~20% of the distance toward the center of the nucleus (Fig. 5 *D*, *iii*). Thus, A3F- and A3G-labeled PICs in the nuclei remain near the nuclear periphery.

Capsid Mutations That Alter Core Stability Decrease Nuclear Import of PICs. Previous studies have shown that the K203A mutation in CA results in less stable viral cores, whereas the E128A/R132A double mutation results in more stable viral cores in vitro (23) and in vivo (24). We infected cells with A3F-labeled virus containing WT, less stable (K203A), or more stable (E128A/R132A) CA mutant viruses and observed a significant decrease in viral infectivity, similar to that previously reported (Fig. 6*A*) (23). Although the number of cellular A3F-YFP particles 6 h after infection was within twofold of WT virus for these mutant viruses (Fig. 6*B*), we observed a dramatic decrease in nuclear import of A3F-YFP particles when the viruses had the K203A or the E128A/R132A mutations (54- or 13-fold decrease, respectively; Fig. 6*C*). Earlier, we observed that some A3F-YFP–labeled particles were not associated with Gag-CeFP, suggesting that these signals may be nonviral vesicles (Fig. 1*F*). The fact that almost no A3F-YFP signals were detected in the nuclei of cells infected with the K203A virus preparation suggests that the nonviral A3F-YFP–labeled vesicles do not enter the nucleus.

To further explore the decrease in nuclear import of the core stability mutants, we determined the percentage of cytoplasmic A3F-YFP particles that were associated with the NE (Fig. 6*D*). There was a significant decrease in the percentage of cytoplasmic A3F-YFP particles that were associated with the NE at the 6-h time point for A3F-labeled K203A and E128A/R132A cytoplasmic PICs relative to WT cytoplasmic PICs (8.3- and 2.6-fold decrease, respectively). These results suggested that the core stability mutations decreased cytoplasmic transport of viral PICs to the NE and/or decreased the stable association of the viral PICs with the NE.

Discussion

Two majors findings of our studies are that inhibition of reverse transcription has no impact on the nuclear import of HIV-1 PICs and that CA mutations that alter viral core stability diminished the association of PICs with the NE as well as their nuclear import. The relationship between reverse transcription, nuclear import, and viral uncoating has not been fully elucidated. Recent studies have indicated that viral core uncoating occurs in coordination with reverse transcription (24), and previous studies have suggested a functional link between uncoating and nuclear import (25, 26). Hulme et al. (24) showed that reverse transcription results in alterations in the viral core that render the virus insensitive to TRIM-CypA inhibition as well as the loss of p24 CA from the RTCs/PICs. Our observation that reverse transcription is not required for nuclear import indicates that the viral uncoating event that is associated with reverse transcription is dispensable for nuclear import. Furthermore, because an intact viral core is unlikely to be transported through the nuclear pore, our results suggest that another uncoating event that does not require reverse transcription occurs either before or during nuclear import of PICs.

Some studies have suggested that viral RNA can be detected in the nucleus by biochemical methods and that reverse transcription can be completed in the nucleus (27–29); this study shows that complete inhibition of reverse transcription has little to no effect on the nuclear import of PICs. It was recently suggested that PICs are imported into the nuclei in the absence of a central DNA flap at 10–15% of the efficiency of the wild-type virus and that this residual nuclear import of PICs does not support efficient spreading infection (30). In these studies, nuclear import of PICs was determined by formation of 2-LTR circles. In our studies A3F-YFP–labeled PICs were imported into the nuclei at nearly the same efficiency for WT and RT^- virus, indicating that the central DNA flap is not required for nuclear import of PICs. Together, these results suggest that the absence of a central DNA flap reduces the efficiency of 2-LTR circle formation but not nuclear import of PICs.

We observed that CA stability mutants diminished the association of PICs with the NE and their nuclear import. Recent studies indicate that CA plays an important role in nuclear import (reviewed in ref. 31). It was recently reported that the cyclophilin domain of Nup358 is an isomerase that catalyzes *cis-trans* isomerization of a proline in HIV-1 CA (P90), which facilitates viral core uncoating and nuclear import of PICs (32). We hypothesize that the CA stability mutants directly or indirectly interfere with the CA–Nup358 interaction, or interaction of the CA with another NE associated protein, which reduce association of the PICs with the NE and diminish nuclear import. It is possible that the CA mutants that reduce core stability do

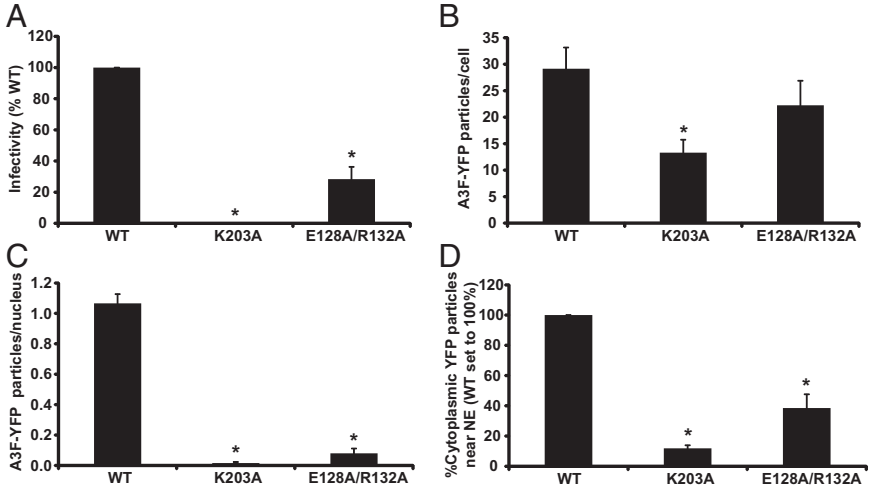

Fig. 6. Capsid mutations that alter core stability decrease nuclear import of A3F-labeled PICs. (*A*) Relative infectivity of A3F-YFP–labeled viruses containing WT, less stable (K203A), or more stable (E128A/R132A) cores. Viruses were used to infect HeLa cells, and the proportion of GFP^+ cells was determined by FACS 48 h after infection. Infectivity was then normalized to p24 CA input. (*B*) Quantitation of the A3F-YFP–labeled particles in the entire cell. HeLa cells were infected with a normalized number of A3F-labeled particles and fixed at 6 h. Confocal z-stacks were acquired of the entire cells, and the YFP signals were quantified. (*C*) Quantitation of the A3F-YFP signals in the nuclei of infected cells. (*D*) The relative percentage of cytoplasmic A3F-YFP particles that was associated with the NE (WT set to 100%). An average of 1,100 particles from 306 cells was analyzed per sample. Error bars indicate the SD of four independent experiments. *Significantly different from WT ($P \leq 0.05$; *t* test).

not interact with the NE because of dissociation of most or all of CA from the PIC; in addition, it is possible that the CA mutants that increase core stability do not undergo a conformational change that is required for association of the PIC with the NE. In our studies the proposed CA–Nup358 interaction, and the resultant CA uncoating, was not affected by inhibition of reverse transcription. Our results suggest that these reverse transcription-associated alterations in the viral core are more subtle compared with the stability mutants in CA analyzed in this study, and do not influence the association of the PICs with the NE or their nuclear import.

A third major outcome of these studies is that A3F-YFP labeling of PICs can provide a valuable tool for analyzing the early stage of HIV-1 infection. The use of GFP-Vpr for analysis of viral postentry events, pioneered by Hope and colleagues (33), has provided numerous valuable insights into postentry events during HIV-1 replication (22, 24, 34–36). However, GFP-Vpr dissociates from the RTCs/PICs shortly after infection and has not been observed in the nuclei of infected cells (33, 36, 37). To date, only a small number of studies have detected PICs in the nuclei of infected cells by using virions labeled with fluorescently tagged IN (38–41), and one recent study showed that there are nuclear IN complexes that are not associated with viral cDNA (42), suggesting that fluorescently tagged IN may not be a suitable marker for labeling PICs in the nuclei. Analysis of the nuclear import of PICs has largely relied on quantification of 2-LTR circles, which requires completion of reverse transcription (43). The fact that A3F-labeled PICs can be visualized in the nuclei, coupled with the fact that reverse transcription is not required for nuclear import, makes it possible to analyze the effects of mutations in viral proteins on nuclear import, independent of their effects on reverse transcription and viral replication. For example, the CA stability mutations analyzed in this study are replication defective and synthesize lower levels of viral DNA and 2-LTR circles (23); therefore, the effect of these mutations on nuclear import could not previously be determined.

We have used A3F-YFP labeling of RTCs/PICs as a tool to develop two assays for analysis of the early stage of HIV-1 replication. First, we established a quantitative assay for stable association of the cytoplasmic viral PICs with the NE and observed that CA stability mutants were defective in either cytoplasmic transport of PICs or their stable association with the NE. Using this assay, mutations in viral or host proteins can be analyzed for their effects on stable association of the PICs with the NE. Future studies using live-cell microscopy could allow analysis of viral and host mutations for their influence on cytoplasmic transport. We also developed an assay to quantify the nuclear penetration distance for PICs and found that the PICs were not distributed throughout the nucleus, traversing on average only ~1.2–1.6 microns from the NE. Interestingly, the distribution of PICs in the nuclei was similar to the recently reported distribution of integrated proviruses (44). Our results and the results of Di Primio et al. (44) suggest that HIV-1 PICs may be transported a short distance into the nuclei, and their location determines their sites of integration.

We observed that A3F-YFP remains associated with the PICs to a greater extent than A3G-YFP through nuclear import. A3F has a higher affinity for dsDNA than A3G (6), and PICs primarily contain dsDNA 6 h after infection (20), which may contribute to A3F's stable association with PICs. The stable association of A3F with PICs is also consistent with our previous observation that A3F inhibits viral replication in part by blocking the 3′ processing step catalyzed by HIV-1 IN (6). Interestingly, the reduced nuclear import of A3F*-YFP–labeled PICs can be partially explained by the lower proportion of NE-associated A3F*-YFP–labeled PICs, indicating that the CD2 domain mutation (E251Q) may lead to a more rapid dissociation of A3F*-YFP from the NE-associated PICs. We observed a fivefold decrease in the number of detectable A3G/A3G*-YFP–labeled particles in cells relative to A3F/A3F*-YFP–labeled particles 3 h after infection, indicating that A3G/A3G*-YFP dissociated from PICs more readily than A3F/A3F*-YFP. It is possible that a fraction of virion-incorporated A3G is located outside of the viral cores, resulting in its dissociation from the cores soon after viral membrane fusion (45). Consistent with our observation that few A3C-YFP–labeled particles remained in the cells at 3 h after infection, A3C was previously reported to be weakly associated with viral cores (46). Interestingly, P22-YFP, which binds to RNA nonspecifically, largely dissociated from the RTCs 3 h after infection, a time point at which reverse transcription is most likely not completed and viral RNA should be present in the RTCs. Additional studies are needed to elucidate the nature of virion incorporation of these proteins and their kinetics of dissociation from RTCs and PICs.

In summary, we have shown that reverse transcription is not required for nuclear import of PICs and that CA mutations that alter the stability of viral cores exhibit defects in stable association with the NE and nuclear import. In addition, we have developed two quantitative assays for stable association of PICs with the NE, and nuclear penetration of PICs, which demonstrate that labeling virions with A3F-YFP, and to a lesser extent A3G-YFP, can provide valuable tools for understanding HIV-1 replication in target cells of infection. Insights in viral replication and virus–host interactions gained through these studies may provide novel targets for future antiviral drug development.

Materials and Methods

Cells, Virus, Infections, and Pharmaceuticals. HeLa and 293T cells were maintained as previously described (47). NVP was obtained through the National Institutes of Health (NIH) AIDS Reagent Program, Division of AIDS, National Institute of Allergy and Infectious Diseases, NIH. DAPI and aphidicolin were obtained from Sigma-Aldrich.

All viruses were prepared by using pHDV-EGFP, which expresses HIV-1 Gag-Pol and EGFP but does not express Env, Vif, Vpr, Vpu, or Nef (48), and were pseudotyped with VSV-G (49). Details of the generation of the HDV-EGFP mutants, the S15-mCherry membrane marker (36), and YFP-tagged protein expression plasmids are provided in *SI Materials and Methods*.

Transfections were carried out using polyethylenimine transfection reagent (Sigma), as previously described (50, 51). Briefly, 3.5×10^6 293T cells were seeded onto 10-cm-diameter dishes and cotransfected the next day with an HDV-EGFP (10 μg), S15-mCherry (5 μg), HCMV-G (VSV-G; 2 μg), and either A3F-YFP (1.25 μg), A3F-E251Q-YFP (5 μg; referred to as A3F*-YFP), A3G-YFP (10 μg), A3G-E259Q-YFP (5 μg; referred to as A3G*-YFP), A3C-YFP (10 μg), or P22-YFP (5 μg). The supernatant containing virus was collected 18 h after transfection, filtered (0.45 μm), and concentrated by ultracentrifugation (100,000 × *g*, 1.5 h, 4 °C) through a 20% sucrose cushion, and resuspended in either PBS or culture medium. For the production of noninfectious, Gag- CeFP–labeled viruses, the same plasmids described above were used, except pHDV-EGFP was replaced with a mixture of pGagCeFP-BglSL (5 μg) and pGag-BglSL (5 μg) (11).

HeLa cells were seeded onto IbiTreated μ-slides (3×10^4 cells per well) and challenged the next day with ~4.5×10^7 YFP particles (as determined by single-virion analysis; see below) in the presence of polybrene (10 μg/mL) at 1,200 × *g* for 1 h at 15 °C, a temperature that permitted virion binding to cell membranes but prevented virion endocytosis (52). After centrifugation the media was replaced with prewarmed media to allow entry into the cells (defined as the 0-h time point) and thereafter incubated at 37 °C. The infected cells were fixed at various time points with 4.0% (wt/vol) paraformaldehyde (PFA) dissolved in 1× PBS. To determine infectivity, the percentage of GFP^+ cells was determined by FACS and then normalized to the p24 CA amount, as determined by ELISA (XpressBio).

Quantitative PCR. Early (RU5) and late (U5Ψ) reverse transcription products, 2-LTR circles, and the host gene *CCR5* (for normalization; 2 *CCR5* copies per cell) were detected by quantitative PCR as previously described (53). The cells were infected at various time points, cellular and viral DNA was extracted from the cells using the QIAamp DNA Blood Mini Kit (Qiagen), and the extracted DNA was treated with DpnI (37 °C for 1 h) to reduce plasmid DNA contamination. Heat-inactivated virus (65 °C for 1 h) was used to infect cells in parallel to determine the level of contamination with plasmid DNA.

siRNA Knockdown. The HeLa cells were reverse-transfected with siRNA targeting Nup153, TNPO3, or nontargeting siRNA (14) using RNAiMax (Invitrogen). Briefly, siRNA and Opti-MEM (Invitrogen) containing RNAiMAX was added to each well and incubated for 30 min. HeLa cells (3×10^4) in an equal volume of Opti-MEM plus 20% (vol/vol) FCS were added to the well and incubated at 37 °C for 48 h (40-nM final concentration of siRNA). Nup153 and TNPO3 were detected in cell lysates by SDS/PAGE and Western blot analysis using anti-nuclear protein complex (Abcam) and anti-TNPO3 (Abcam) antibodies, respectively, as previously described (47).

Immunofluorescence Staining and FISH. For immunofluorescence staining, cells were permeabilized with 0.25% Triton X-100 for 10 min and blocked for 45 min with PBS containing 0.1% Triton X-100 (PBST) and 3% (wt/vol) BSA (PBST/BSA). To detect the NE, cells were incubated with an anti-Lamin A/C antibody (Pierce) for 1 h, followed by incubation with an Alexa Fluor 405-labeled secondary antibody (Invitrogen) for 30 min. For dual immunofluorescence staining and FISH for the detection of the NE and viral RNA, respectively, cells were permeabilized with 0.25% Triton X-100 for 10 min in the presence of the RNase inhibitor 2 mM ribonucleoside-vanadyl complex (RVC; New England Biolabs) and blocked with blocking buffer [1% RNase-free BSA (Life Technologies) in PBS plus 2 mM RVC] for 45 min. To detect the NE, the cells were incubated with an anti-Lamin A/C antibody for 1 h, followed by incubation with an Alexa Fluor 405-labeled secondary antibody for 30 min. The cells were fixed again with 4.0% (wt/vol) PFA for 10 min and then washed with wash buffer [2× SSC, 10% (vol/vol) formamide, RNase-free H_20, and 2 mM RVC]. To detect viral RNA, cells were incubated with a set of 48 unique CalFluor610-labeled Stellaris probes (Biosearch Technologies) that specifically bind *gag-pol* in HIV-1 RNA that were diluted in hybridization buffer [2× SSC, 10% (vol/vol) formamide, 10% (wt/vol) dextran sulfate, and 2 mM RVC] for 4 h at 37 °C. The cells were washed once with wash buffer for 30 min at 37 °C and then washed twice with 2× SSC and stored in 2× SSC until imaging.

Microscopy and Image Analysis. Single-virion analysis was performed as previously described (11, 47), with minor modification. Briefly, a small amount of concentrated virus (0.4 μL) was diluted in PBS and centrifuged onto Ibi-Treated μ-slides (Ibidi) at 1200 × *g* for 1 h. Epifluorescence microscopy was performed with an inverted Nikon Eclipse T*i* microscope and a 100× N.A.-1.40 oil objective, using an X-Cite 120 system (EXFO Photonic Solution) for illumination. Fourteen-bit digital images were acquired sequentially for each channel using an iXon3 897 camera (Andor) with the excitation and emission filter sets 430/24 nm and 480/40 nm for CeFP, 504/12 nm and 542/27 nm for YFP, and 577/25 nm and 650/75 nm for mCherry. The number, positions, and integrated intensities of the diffraction-limited spots were measured for each channel using Localize (54). The positions of the spots were also used to determine colocalization; spots were considered colocalized if the centers of the spots were within 3 pixels. The number of YFP particles detected per field of view is representative of the amount of labeled virus in the virus preparation (47) and was used to estimate the number of YFP particles in each virus preparation.

Confocal z-stacks were acquired of the entire cells using an LSM710 laser scanning confocal microscope (Zeiss) equipped with 405-nm, 515-nm, 561-nm, and 594-nm lasers and a Plan-Apochromat 63× N.A.-1.40 oil objective using a step size of 0.5 μm. The YFP particles inside each nucleus were counted using intensity thresholds based on mock-infected cells. The HIV-1 RNA particles inside each nucleus were counted using intensity thresholds based on mock-infected cells that were probed for HIV-1 RNA. For determining the average number of particles per cell the confocal z-stacks were merged into a maximum image projection, and the number and positions of the spots for each channel were calculated using Localize. The number of particles was then divided by the number of cells in each frame (15–20 cells per frame) to obtain an average number of particles per cell.

Assays to Determine Stable Association of PICs with the NE and Nuclear Penetration of PICs. To determine the percentage of cytoplasmic particles that were near the NE, a single slice located approximately half-height of the nucleus was exported from each confocal z-stack. The YFP particles were detected in each frame using Localize, and a new image was created using the Localize output (particles are represented by a single pixel at the center of each diffraction-limited spot). The new YFP image and the image of the NE were imported into MetaXpress 5.1 (MetaMorph-based software). A ring 4 pixels in width (~1.0 μm) that includes the area on and immediately surrounding the NE was created. For each frame, the percentage of cytosolic YFP particles that were on or near the NE (i.e., colocalized with mask of NE region) was determined. To estimate area of the NE mask relative to the area of the cytoplasm, we divided the area of the cytoplasm [which was calculated by subtracting the total area of the nuclei (excluding NE) from the total area of the frame] by the area of the NE mask for each frame. Because we have no cytoplasmic stain, only frames in which there were >20 cells were used for the analysis, because most of the area of the frame outside the nuclei would contain cytoplasm and not empty space. Frames that contained <20 cells, and likely contained areas without cells, were excluded to avoid an overestimation of the cytoplasmic area.

To determine the distance each YFP particle traveled into the nucleus, a series of 9 rings (2 pixels wide; 0.53 μm) inside each nucleus was created starting from the inside edge of the NE toward the center of the nucleus. The YFP particles in each ring were quantified.

Statistical Analysis. An unpaired Student *t* test was performed to assess whether the differences between samples were significant; *P* values ≤0.05 indicated statistical significance.

ACKNOWLEDGMENTS. We thank Krista Delviks-Frankenberry and Maria Hamscher for construction of CA mutants, Stephen Lockett and De Chen (Optical Microscopy and Image Analysis Laboratory, Leidos Biomedical Research, Inc.) for use of the Zeiss LSM710 confocal microscope and help with data analysis, Dan Larson for providing Localize, and Sergey Plisov for help with data analysis. This research was supported in part by the Intramural Research Program of the National Institutes of Health, Center for Cancer Research, National Cancer Institute.

1. Smith JL, Bu W, Burdick RC, Pathak VK (2009) Multiple ways of targeting APOBEC3-virion infectivity factor interactions for anti-HIV-1 drug development. *Trends Pharmacol Sci* 30(12):638–646.
2. Sheehy AM, Gaddis NC, Choi JD, Malim MH (2002) Isolation of a human gene that inhibits HIV-1 infection and is suppressed by the viral Vif protein. *Nature* 418(6898):646–650.
3. Zheng YH, et al. (2004) Human APOBEC3F is another host factor that blocks human immunodeficiency virus type 1 replication. *J Virol* 78(11):6073–6076.
4. Yu Q, et al. (2004) APOBEC3B and APOBEC3C are potent inhibitors of simian immunodeficiency virus replication. *J Biol Chem* 279(51):53379–53386.
5. Mbisa JL, et al. (2007) Human immunodeficiency virus type 1 cDNAs produced in the presence of APOBEC3G exhibit defects in plus-strand DNA transfer and integration. *J Virol* 81(13):7099–7110.
6. Mbisa JL, Bu W, Pathak VK (2010) APOBEC3F and APOBEC3G inhibit HIV-1 DNA integration by different mechanisms. *J Virol* 84(10):5250–5259.
7. Brown PO, Bowerman B, Varmus HE, Bishop JM (1989) Retroviral integration: Structure of the initial covalent product and its precursor, and a role for the viral IN protein. *Proc Natl Acad Sci USA* 86(8):2525–2529.
8. Austin RJ, Xia T, Ren J, Takahashi TT, Roberts RW (2003) Differential modes of recognition in N peptide-boxB complexes. *Biochemistry* 42(50):14957–14967.
9. Tan R, Frankel AD (1995) Structural variety of arginine-rich RNA-binding peptides. *Proc Natl Acad Sci USA* 92(12):5282–5286.
10. Friew YN, Boyko V, Hu WS, Pathak VK (2009) Intracellular interactions between APOBEC3G, RNA, and HIV-1 Gag: APOBEC3G multimerization is dependent on its association with RNA. *Retrovirology* 6:56.
11. Chen J, et al. (2009) High efficiency of HIV-1 genomic RNA packaging and heterozygote formation revealed by single virion analysis. *Proc Natl Acad Sci USA* 106(32):13535–13540.
12. De Iaco A, Luban J (2011) Inhibition of HIV-1 infection by TNPO3 depletion is determined by capsid and detectable after viral cDNA enters the nucleus. *Retrovirology* 8:98.
13. Lee K, et al. (2010) Flexible use of nuclear import pathways by HIV-1. *Cell Host Microbe* 7(3):221–233.
14. Matreyek KA, Engelman A (2011) The requirement for nucleoporin NUP153 during human immunodeficiency virus type 1 infection is determined by the viral capsid. *J Virol* 85(15):7818–7827.
15. Shah VB, et al. (2013) The host proteins transportin SR2/TNPO3 and cyclophilin A exert opposing effects on HIV-1 uncoating. *J Virol* 87(1):422–432.
16. Julias JG, Ferris AL, Boyer PL, Hughes SH (2001) Replication of phenotypically mixed human immunodeficiency virus type 1 virions containing catalytically active and catalytically inactive reverse transcriptase. *J Virol* 75(14):6537–6546.
17. Fricke T, et al. (2013) The ability of TNPO3-depleted cells to inhibit HIV-1 infection requires CPSF6. *Retrovirology* 10:46.
18. Valle-Casuso JC, et al. (2012) TNPO3 is required for HIV-1 replication after nuclear import but prior to integration and binds the HIV-1 core. *J Virol* 86(10):5931–5936.
19. Di Nunzio F, et al. (2012) Human nucleoporins promote HIV-1 docking at the nuclear pore, nuclear import and integration. *PLoS One* 7(9):e46037.
20. Thomas DC, et al. (2007) Determination of the ex vivo rates of human immunodeficiency virus type 1 reverse transcription by using novel strand-specific amplification analysis. *J Virol* 81(9):4798–4807.
21. Pedrali-Noy G, Spadari S (1980) Aphidicolin allows a rapid and simple evaluation of DNA-repair synthesis in damaged human cells. *Mutat Res* 70(3):389–394.
22. Yamashita M, Perez O, Hope TJ, Emerman M (2007) Evidence for direct involvement of the capsid protein in HIV infection of nondividing cells. *PLoS Pathog* 3(10):1502–1510.

23. Forshey BM, von Schwedler U, Sundquist WI, Aiken C (2002) Formation of a human immunodeficiency virus type 1 core of optimal stability is crucial for viral replication. *J Virol* 76(11):5667–5677.
24. Hulme AE, Perez O, Hope TJ (2011) Complementary assays reveal a relationship between HIV-1 uncoating and reverse transcription. *Proc Natl Acad Sci USA* 108(24): 9975–9980.
25. Arhel NJ, et al. (2007) HIV-1 DNA Flap formation promotes uncoating of the pre-integration complex at the nuclear pore. *EMBO J* 26(12):3025–3037.
26. Dismuke DJ, Aiken C (2006) Evidence for a functional link between uncoating of the human immunodeficiency virus type 1 core and nuclear import of the viral preintegration complex. *J Virol* 80(8):3712–3720.
27. Bukrinsky MI, et al. (1993) Association of integrase, matrix, and reverse transcriptase antigens of human immunodeficiency virus type 1 with viral nucleic acids following acute infection. *Proc Natl Acad Sci USA* 90(13):6125–6129.
28. Iordanskiy S, Berro R, Altieri M, Kashanchi F, Bukrinsky M (2006) Intracytoplasmic maturation of the human immunodeficiency virus type 1 reverse transcription complexes determines their capacity to integrate into chromatin. *Retrovirology* 3:4.
29. Zaitseva L, et al. (2009) HIV-1 exploits importin 7 to maximize nuclear import of its DNA genome. *Retrovirology* 6:11.
30. Iglesias C, et al. (2011) Residual HIV-1 DNA Flap-independent nuclear import of cPPT/CTS double mutant viruses does not support spreading infection. *Retrovirology* 8:92.
31. Fassati A (2012) Multiple roles of the capsid protein in the early steps of HIV-1 infection. *Virus Res* 170(1-2):15–24.
32. Bichel K, et al. (2013) HIV-1 capsid undergoes coupled binding and isomerization by the nuclear pore protein NUP358. *Retrovirology* 10:81.
33. McDonald D, et al. (2002) Visualization of the intracellular behavior of HIV in living cells. *J Cell Biol* 159(3):441–452.
34. Campbell EM, Hope TJ (2008) Live cell imaging of the HIV-1 life cycle. *Trends Microbiol* 16(12):580–587.
35. Campbell EM, Perez O, Anderson JL, Hope TJ (2008) Visualization of a proteasome-independent intermediate during restriction of HIV-1 by rhesus TRIM5alpha. *J Cell Biol* 180(3):549–561.
36. Campbell EM, Perez O, Melar M, Hope TJ (2007) Labeling HIV-1 virions with two fluorescent proteins allows identification of virions that have productively entered the target cell. *Virology* 360(2):286–293.
37. Xu H, et al. (2013) Evidence for biphasic uncoating during HIV-1 infection from a novel imaging assay. *Retrovirology* 10:70.
38. Albanese A, Arosio D, Terreni M, Cereseto A (2008) HIV-1 pre-integration complexes selectively target decondensed chromatin in the nuclear periphery. *PLoS One* 3(6): e2413.
39. Arhel N, et al. (2006) Quantitative four-dimensional tracking of cytoplasmic and nuclear HIV-1 complexes. *Nat Methods* 3(10):817–824.
40. Christ F, et al. (2008) Transportin-SR2 imports HIV into the nucleus. *Curr Biol* 18(16): 1192–1202.
41. Lelek M, et al. (2012) Superresolution imaging of HIV in infected cells with FlAsH-PALM. *Proc Natl Acad Sci USA* 109(22):8564–8569.
42. Gérard A, Soler N, Ségéral E, Belshan M, Emiliani S (2013) Identification of low molecular weight nuclear complexes containing integrase during the early stages of HIV-1 infection. *Retrovirology* 10:13.
43. Butler SL, Hansen MS, Bushman FD (2001) A quantitative assay for HIV DNA integration in vivo. *Nat Med* 7(5):631–634.
44. Di Primio C, et al. (2013) Single-cell imaging of HIV-1 provirus (SCIP). *Proc Natl Acad Sci USA* 110(14):5636–5641.
45. Song C, Sutton L, Johnson ME, D'Aquila RT, Donahue JP (2012) Signals in APOBEC3F N-terminal and C-terminal deaminase domains each contribute to encapsidation in HIV-1 virions and are both required for HIV-1 restriction. *J Biol Chem* 287(20): 16965–16974.
46. Zhang W, et al. (2010) Association of potent human antiviral cytidine deaminases with 7SL RNA and viral RNP in HIV-1 virions. *J Virol* 84(24):12903–12913.
47. Burdick R, et al. (2010) P body-associated protein Mov10 inhibits HIV-1 replication at multiple stages. *J Virol* 84(19):10241–10253.
48. Unutmaz D, KewalRamani VN, Marmon S, Littman DR (1999) Cytokine signals are sufficient for HIV-1 infection of resting human T lymphocytes. *J Exp Med* 189(11): 1735–1746.
49. Yee JK, Friedmann T, Burns JC (1994) Generation of high-titer pseudotyped retroviral vectors with very broad host range. *Methods Cell Biol* 43(Pt A):99–112.
50. Boussif O, et al. (1995) A versatile vector for gene and oligonucleotide transfer into cells in culture and in vivo: Polyethylenimine. *Proc Natl Acad Sci USA* 92(16): 7297–7301.
51. Russell RA, Smith J, Barr R, Bhattacharyya D, Pathak VK (2009) Distinct domains within APOBEC3G and APOBEC3F interact with separate regions of human immunodeficiency virus type 1 Vif. *J Virol* 83(4):1992–2003.
52. O'Doherty U, Swiggard WJ, Malim MH (2000) Human immunodeficiency virus type 1 spinoculation enhances infection through virus binding. *J Virol* 74(21):10074–10080.
53. Mbisa JL, Delviks-Frankenberry KA, Thomas JA, Gorelick RJ, Pathak VK (2009) Real-time PCR analysis of HIV-1 replication post-entry events. *Methods Mol Biol* 485:55–72.
54. Zenklusen D, Larson DR, Singer RH (2008) Single-RNA counting reveals alternative modes of gene expression in yeast. *Nat Struct Mol Biol* 15(12):1263–1271.